



Cite this: *Chem. Commun.*, 2019, 55, 334

Received 12th November 2018,
Accepted 4th December 2018

DOI: 10.1039/c8cc08992b

rsc.li/chemcomm

Boosting oxygen reduction activity with low-temperature derived high-loading atomic cobalt on nitrogen-doped graphene for efficient Zn–air batteries†

Jiantao Li,‡ Haoyun Liu,‡ Manman Wang,‡ Chao Lin, Wei Yang, Jiashen Meng, Yanan Xu, Kwadwo Asare Owusu, Benli Jiang, Chuanxi Chen, Danian Fan, Liang Zhou * and Liqiang Mai *

High-loading atomic cobalt (12.8 wt%) dispersed on nitrogen-doped graphene was successfully synthesized via considerably low temperature pyrolysis. The catalyst exhibits excellent electrocatalytic performance towards the oxygen reduction reaction with a large limiting diffusion current density of 5.60 mA cm⁻² (10% higher than that of commercial Pt/C), and when acting as the air catalyst of Zn–air batteries, a high open-circuit voltage of >1.40 V and excellent power density are also achieved.

The oxygen reduction reaction (ORR) is one of the most fundamental and important reactions in fuel cells and metal–air batteries.^{1,2} However, this reaction suffers from slow kinetics, and thus highly efficient electrocatalysts are required to promote the reaction processes.^{2,3} Platinum-based catalysts are the most active ORR catalysts, but scarcity and high cost limit their widespread use.¹ In this regard, active, durable and low-cost electrocatalysts are indeed essential for the ORR.

Transition metal single atoms supported on nitrogen-doped-carbon (denoted as single-atom catalysts (SACs)) have emerged as promising alternatives to noble metal-based catalysts due to their high activity in electrocatalysis.^{4,5} Specifically, Zelenay *et al.* developed a kind of highly active Fe–N–C catalyst *via* pyrolyzing a polyaniline/cyanamide-based precursor at 900 °C, and a remarkable ORR performance was achieved.¹ Tour *et al.* designed an electrocatalyst with Co atoms anchored on nitrogen-doped graphene *via* annealing the mixture of an inorganic salt and graphene at 750 °C in NH₃, obtaining efficient electrocatalytic performance towards the hydrogen evolution reaction.⁶ Zhang *et al.* also reported a self-supporting Co–N–C catalyst for hydrogenation of nitroarenes through 700 °C pyrolysis of a Co(phen)₂(OAc)₂ complex precursor.⁷

For SACs, the active site number and specific activity (normalized by surface area) will both increase when the metal loading goes up, while atoms will easily aggregate into nanoparticles if the loading reaches a certain amount.⁸ Besides, most of the SACs are synthesized through high temperature pyrolysis (>700 °C), making high energy consumption inevitable. Thus, how to obtain SACs with high-loading *via* low temperature still remains a challenge.

In this work, we report a low temperature method (300 to 400 °C) to disperse the cobalt atoms on nitrogen-doped graphene (denoted as CoNG) *via* thermal treatment under flowing NH₃ atmosphere. The nitrogen species as well as cobalt states of CoNG have been mainly tuned through controlling the temperature. CoNG-350 exhibits optimal performance in the ORR, and primary Zn–air batteries based on CoNG-350 as the air catalyst show high power density and good operation durability.

The synthesis process of CoNG is schematically illustrated in Fig. S1 (ESI†). A precursor solution containing cobalt acetate and graphene oxide was freeze-dried to obtain a brownish cotton-like sample, and then the final product (Co dispersed on nitrogen-doped graphene, CoNG) was achieved through annealing the dried sample under flowing NH₃ atmosphere with considerably much lower temperature (300 °C to 400 °C) compared with other reported works (summarized in Table S1, ESI†). Controlled samples with different Co loading on nitrogen-doped graphene (NG, Co_{0.5}NG and Co₃NG) were also synthesized through the same procedure except that the amount of cobalt acetate added in the precursor solution was different. It should be pointed out that the synthetic procedure is significantly different from that reported by Tour *et al.*⁶ The annealing temperature is much lower (high temperature pyrolysis is usually inevitable to obtain high performance M–N–C catalysts)⁸ and the metal loading is much higher (higher metal loading will result in higher activity especially for metal single atom catalysts).⁹

Scanning electron microscopy (SEM) and transmission electron microscopy (TEM) images of CoNG-350 are shown in

State Key Laboratory of Advanced Technology for Materials Synthesis and Processing, International School of Materials Science and Engineering, Wuhan University of Technology, Wuhan 430070, Hubei, China.
E-mail: liangzhou@whut.edu.cn, mlq518@whut.edu.cn

† Electronic supplementary information (ESI) available. See DOI: 10.1039/c8cc08992b

‡ These authors contributed equally to this work.

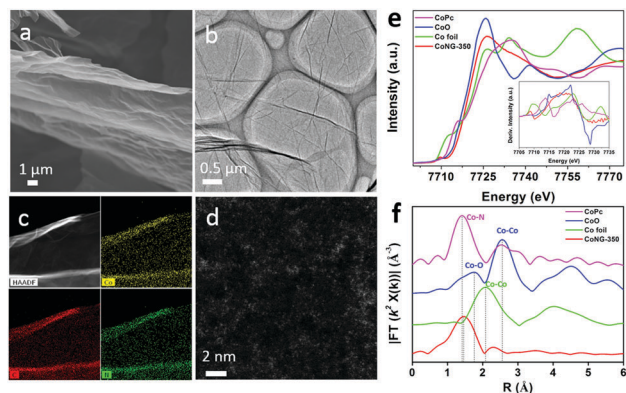


Fig. 1 (a) SEM and (b) TEM images of CoNG-350; (c) HAADF-STEM image and the corresponding EDX elemental maps of CoNG-350; (d) HR HAADF-STEM image of CoNG-350; (e) Co K-edge XANES spectra and (f) Fourier-transformed EXAFS spectra of CoNG-350 and its reference samples, and inset in (e) is the first derivative XANES data.

Fig. 1a and b, respectively. Graphene-like morphology is kept after annealing, and no impurities can be observed. NG-350, CoNG-300 and CoNG-400 also exhibit the same morphology as CoNG-350 (Fig. S2a–d, ESI†). From the high-angle annular dark field scanning transmission electron microscopy (HAADF-STEM) image and corresponding energy-dispersive X-ray (EDX) elemental maps of CoNG-350 (Fig. 1c), it can be seen that the elements of Co, C and N are uniformly dispersed. The high-resolution (HR) HAADF-STEM image (Fig. 1d) further demonstrates that a number of bright spots corresponding to Co species are homogeneously dispersed on graphene.

To further verify the coordination structure and chemical state of Co in CoNG-350, X-ray absorption fine structure (XAFS) analysis at the Co K-edge was carried out. Co K-edge X-ray absorption near-edge structure (XANES) spectra of CoNG-350 as well as the reference samples are shown in Fig. 1e. The XANES profile of CoNG-350 is different from those of the reference samples. Specifically, a pre-edge peak at ~ 7715 eV of CoPc can be observed, which is assigned to the Co-N₄ square-planar structure,⁷ but the pre-edge peak of CoNG-350 is located at ~ 7710 eV, which is indicative of forbidden 1s-to-3d transition in the octahedral configuration.^{10,11} The first derivative XANES data (inset in Fig. 1e) shows that the energy value at the first inflection point of the XANES spectra is about 7720, 7709, 7720 and 7721 eV for CoNG-350, Co foil, CoO and CoPc, respectively, suggesting that the CoNG-350 has a Co valence state of about +2.^{5,7} The Fourier-transformed extended X-ray absorption fine structure (EXAFS) spectra (Fig. 1f) are also shown in *R* space without phase correction (the *R* value is not the actual distance between atoms). The main peaks of Co–Co and Co–O in Co foil and CoO exhibit longer *R* distance than that of CoNG-350, indicating that no metallic Co and cobalt oxide-like species exist in CoNG-350.⁷ Meanwhile, the prominent peak of CoNG-350 located at 1.44 Å is very close to that of cobalt phthalocyanine (CoPc) (1.41 Å), demonstrating the possible configuration of Co–N₄ in CoNG-350, and considering the octahedral feature deduced from the pre-edge peak, it is further inferred that two

oxygen molecules may also be adsorbed on the Co center along the vertical direction.^{7,10,11} Based on the above analysis and the previous reports,^{6,7,12} it can be concluded that Co is atomically dispersed on N-doped graphene, and shows a valence state of about +2 with N in the first coordination shell.

Chemical composition and elemental state were further characterized by X-ray photoelectron spectroscopy (XPS). The XPS survey spectra (Fig. S4a, ESI†) show the presence of C, N, O and Co in all CoNG samples annealed at different temperatures. By combining inductively coupled plasma optical emission spectrometry (ICP-OES) and CHNO elemental analysis, the elemental content of CoNG-350 is determined (Fig. S4b, ESI†), and the Co loading is measured to be 2.89 at% (12.8 wt%). The Co loading of CoNG-300 (2.65 at%) and CoNG-400 (2.72 at%) is almost as high as that of CoNG-350 (Fig. S4e, ESI†). It is noted that the Co loading in CoNG is much higher than those of previous reports (summarized in Table S1, ESI†). Specifically, the Co content in CoNG-350 is 235% as much as that reported by Tour *et al.*⁶ who used a similar method to synthesize Co–N–G *via* much higher temperature pyrolysis. The reason for such a high loading of atomic Co is that the pyrolysis temperature is low enough and Co species do not easily aggregate, thus, a higher feeding ratio of Co source can be added without danger of forming nanoparticles.

The O 1s XPS spectra (Fig. S4c, ESI†) of all the samples are deconvoluted into three peaks at 530.3, 531.4 and 533.3 eV, ascribed to C=O, C–O and C–OH, respectively,¹³ and the C 1s XPS spectra also present the corresponding bonds connected to oxygen or nitrogen in all samples (Fig. S4d, ESI†).⁶ The absence of Co–O peaks indicates that there is no coordination between cobalt and oxygen, *i.e.*, no cobalt oxide-like species are formed. The Raman spectra (Fig. S3, ESI†) reflect that the intensity ratio of the D-band (band for disorder, 1325 cm^{−1}) to G-band (band for graphite, 1590 cm^{−1}) changes with temperature, and CoNG-350 has the lowest value of I_D/I_G , suggesting that the sample annealed at 350 has a better graphitic structure, which can facilitate the electron transfer during ORR processes.¹⁴

The N 1s XPS spectra (Fig. 2a) can be deconvoluted into different types of nitrogen, namely Co–N/pyridinic N (398.4 eV; the binding energy between Co–N and pyridinic N are too close to be deconvoluted), pyrrolic N (399.6 eV) and graphitic N (401.3 eV).^{12,15} It has been widely demonstrated that pyridinic N plays a crucial role in ORR performance, and a higher proportion of pyridinic N can result in more efficient catalytic performance towards the ORR.^{2,16} As shown in Fig. 2b, with the temperature increasing from 300 to 400 °C, the content of graphitic N rises while pyrrolic N decreases, and an extreme value of pyridinic N content appears at 350 °C.

The Co 2p XPS spectra (Fig. 2c) of all the samples show two peaks located at ~ 796.5 and ~ 781.1 eV, corresponding to 2p_{1/2} and 2p_{3/2} levels, respectively.^{6,17} The binding energy difference of the two peaks above is ~ 15.4 eV, which is characteristic of Co(II) species,¹⁷ and the result is consistent with that observed from XANES data. The enlarged region of the Co 2p_{3/2} XPS spectra (Fig. 2d) presents a slight decrease of binding energy with the increase of temperature, revealing that more electrons

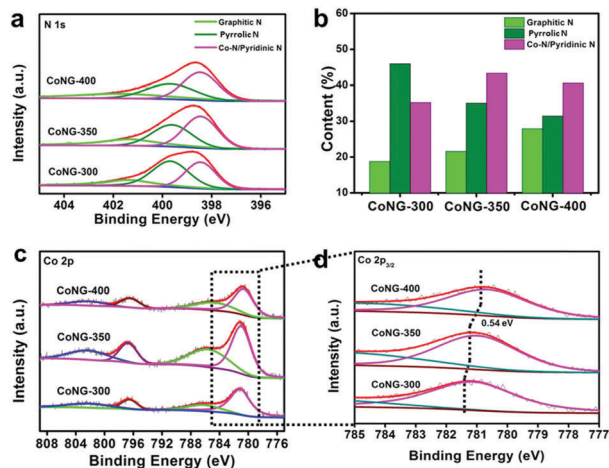


Fig. 2 XPS spectra analysis of CoNG-300, CoNG-350 and CoNG-400: (a) high-resolution N 1s XPS spectra and (b) percentages of different types of N analyzed from (a); (c) high-resolution Co 2p_{3/2} XPS spectra and (d) the corresponding enlargement of (c).

accumulate around the local Co atom's center, and the higher electron density around Co atom sites can promote the electron consuming processes of the ORR.

Electrocatalytic performance for the ORR of all the as-synthesized samples and state-of-the-art commercial Pt/C (20 wt%) were measured on a rotating disk electrode (RDE) in O₂-saturated 0.1 M KOH. Fig. 3a shows the typical cyclic voltammograms (CVs) at the scan rate of 5 mV s⁻¹. CoNG samples annealed at different temperatures show more positive cathodic peaks than that of NG-350 (0.70 V), indicating the importance of dispersing Co atoms on NG. Besides, CoNG-350 possesses a more positive peak value (0.82 V) than CoNG-300 (0.80 V) and CoNG-400 (0.81 V), suggesting that the sample annealed at 350 °C has the best performance. Linear sweep voltammetry (LSV) curves (Fig. 3b) reveal that CoNG-350 has the highest onset potential (0.90 V) and limiting diffusion current density (5.60 mA cm⁻²) among all the as-synthesized samples, and the limiting current density of CoNG-350 is even higher than that of commercial Pt/C (5.1 mA cm⁻²) and recently reported single-atom catalysts (summarized in Table S1, ESI[†]).

The Tafel plots based on specific activity (Fig. 3c) exhibit a slope of 54, 50, 51, 86 and 89 mV dec⁻¹ for CoNG-300, CoNG-350, CoNG-400, NG-350 and Pt/C, respectively. A smaller slope achieved in CoNG-350 suggests considerably faster kinetics for the ORR.^{3,18} Koutecky–Levich (K–L) curves (Fig. S6b, ESI[†]) derived from the ORR polarization curves (Fig. S6a, ESI[†]) confirm the 4-electron transfer reaction of the ORR using CoNG-350 as the catalyst. To further investigate the electron-transfer number and the hydrogen peroxide yield (H₂O₂⁻%), rotating ring-disk electrode (RRDE) measurements were also carried out for CoNG-350 and Pt/C catalysts (Fig. 3d). The electron transfer number and the peroxide yield for CoNG-350 are close to 4 and 4%, respectively, at the region of 0.45–0.80 V (Fig. 3e). Chronoamperometric tests at half-wave potential were also carried out (Fig. 3f). CoNG-350 and Pt/C kept 82% and 77% of their initial current after long term running of

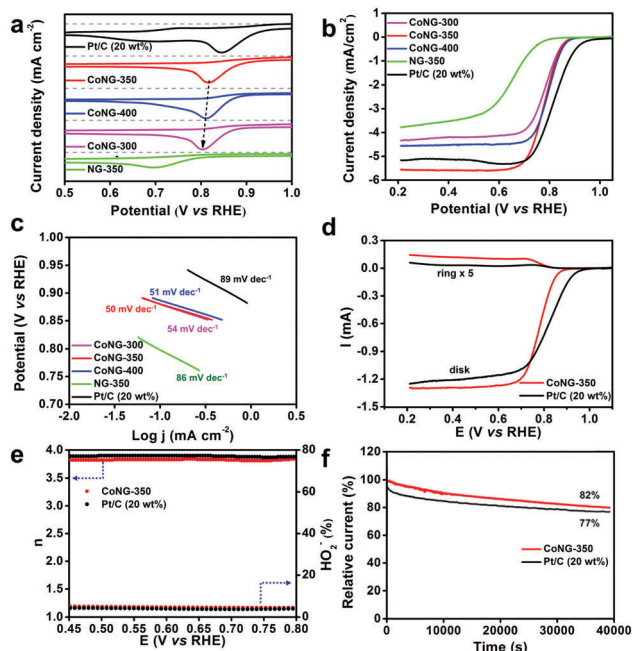


Fig. 3 ORR performance of CoNG-300, CoNG-350, CoNG-400, NG-350 and Pt/C tested in O₂-saturated 0.1 M KOH solution: (a) CV curves tested at the scan rate of 5 mV s⁻¹; (b) LSV curves tested at the rotation speed of 1600 rpm with the scan rate of 5 mV s⁻¹; (c) Tafel plots derived from (b). (d) LSV curves of CoNG-350 and Pt/C measured on RRDE; (e) peroxide yields and electron-transfer numbers of CoNG-350 and Pt/C; (f) chronoamperometric curves measured at half-wave potentials of CoNG-350 and Pt/C.

~40 000 s, respectively, validating the stability during the ORR of CoNG-350.

To study the effect of Co loading on the electrocatalytic performance, we also synthesized Co_{0.5}NG-350 and Co₃NG-350 for comparison. As shown in Fig. S7a–d (ESI[†]), the surface on graphene is very clean and smooth for Co_{0.5}NG-350, while obvious particles can be observed for Co₃NG-350, suggesting that when the Co content is increased, cobalt species will aggregate without forming single atoms. Both the onset potential and limiting diffusion current density of CoNG-350 are much higher than those of Co_{0.5}NG-350 and Co₃NG-350 (Fig. S7e, ESI[†]), confirming the preferential amount of Co atoms dispersed on NG of CoNG-350.

To illustrate the relationship between high electrocatalytic performance and chemical structure, work function was measured by ultraviolet photoelectron spectroscopy (UPS, Fig. S5, ESI[†]): the lower the value of the work function is, the easier the transfer of electrons from catalyst to reactant is.^{16,19,20} CoNG-350 possesses lower work function (5.94 eV) compared with CoNG-300, CoNG-400 and NG-350, revealing that the electrons from CoNG-350 can be more easily stimulated to take part in the processes of ORR. Besides, based on the previous analysis, the sample annealed at 350 °C possesses an optimal content of different types of N, and pyridinic N which benefits the ORR processes has the highest content percentage; the local electron density around Co atom sites of the samples annealed at higher temperature is denser, and the denser electron density can also promote the electron consuming processes of the ORR.

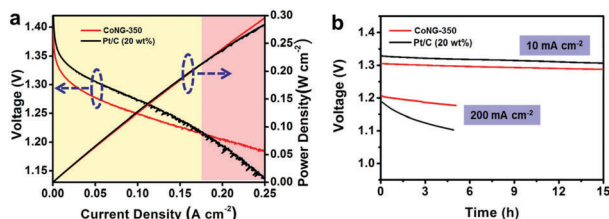


Fig. 4 Electrochemical performance of primary zinc-air batteries. (a) Discharge polarization curves and corresponding power density of CoNG-350 and Pt/C, respectively. (b) Galvanostatic discharge curves of CoNG-350 and Pt/C tested at 10 and 200 mA cm⁻². All the data are *iR* corrected ($R = 1.25 \Omega$).

Encouraged by promising ORR electrochemical results, CoNG-350 was applied as the air catalyst of a primary Zn-air battery, which has attracted great interest over recent years as a kind of promising energy storage device.^{21–23} To assess the battery performance, ink made from CoNG-350 or Pt/C was uniformly deposited onto hydrophobic carbon fiber paper (CFP) as the air cathode (active material loading is 1 mg cm⁻²), and the electrochemical performance was measured in 6 M KOH using a customized electrochemical cell.

Fig. 4a depicts the curves for polarization and power density. The open circuit voltage of the Zn-air battery based on CoNG-350 is >1.40 V, and in the high current density region (>175 mA cm⁻², pink region), the voltage of the CoNG-350 based Zn-air battery is superior to that of the Pt/C based cell. Moreover, the power density can reach 300 mW cm⁻², higher than that of the Pt/C based Zn-air battery. For the CoNG-350 based Zn-air battery, only a slight voltage loss can be observed after galvanostatically discharging at the current density of 10 mA cm⁻² for 15 h (Fig. 4b), close to that of Pt/C. While at 200 mA cm⁻², there is a significant voltage loss for Pt/C, and CoNG-350 is relatively more stable. Moreover, as depicted in Fig. S8 (ESI[†]) the specific discharge capacity of CoNG-350 is 785 mA h g⁻¹, higher than that of Pt/C (760 mA h g⁻¹). The energy density of CoNG-350 is calculated to be 926 W h kg⁻¹, almost the same as that of Pt/C (927 W h kg⁻¹). The above results suggest that CoNG-350 can serve as a robust catalyst for Zn-air batteries due to its high activity and good durability.

In summary, N-doped graphene supported atomic cobalt was feasibly obtained at a considerably low temperature. High activity and robust durability of CoNG-350 for the ORR were achieved, and excellent electrochemical performance of the CoNG-350 based Zn-air battery was also realized. The optimal content of different types of N and the higher electron density around Co atom sites as well as the low work function are responsible for the improved electrocatalytic performance. Our synthetic strategy can be extended to prepare other kinds of non-noble atomic metals supported on N-doped graphene, and the electrochemical performance may be further improved through the control of metal species.

This work was supported by the National Key Research and Development Program of China (2016YFA0202603), the National Natural Science Foundation of China (51521001, 21673171, 51502226) and the National Natural Science Fund for Distinguished Young Scholars (51425204).

Conflicts of interest

There are no conflicts to declare.

Notes and references

- H. T. Chung, D. A. Cullen, D. Higgins, B. T. Sneed, E. F. Holby, K. L. More and P. Zelenay, *Science*, 2017, **357**, 479.
- K. Gong, F. Du, Z. Xia, M. Durstock and L. Dai, *Science*, 2009, **323**, 760.
- M. Li, Z. Zhao, T. Cheng, A. Fortunelli, C.-Y. Chen, R. Yu, Q. Zhang, L. Gu, B. V. Merinov, Z. Lin, E. Zhu, T. Yu, Q. Jia, J. Guo, L. Zhang, W. A. Goddard, Y. Huang and X. Duan, *Science*, 2016, **354**, 1414.
- Y. Chen, S. Ji, Y. Wang, J. Dong, W. Chen, Z. Li, R. Shen, L. Zheng, Z. Zhuang, D. Wang and Y. Li, *Angew. Chem., Int. Ed.*, 2017, **56**, 6937.
- H. Fei, J. Dong, Y. Feng, C. S. Allen, C. Wan, B. Volosskiy, M. Li, Z. Zhao, Y. Wang, H. Sun, P. An, W. Chen, Z. Guo, C. Lee, D. Chen, I. Shakir, M. Liu, T. Hu, Y. Li, A. I. Kirkland, X. Duan and Y. Huang, *Nat. Catal.*, 2018, **1**, 63.
- H. Fei, J. Dong, M. J. Arellano-Jiménez, G. Ye, N. Dong Kim, E. L. G. Samuel, Z. Peng, Z. Zhu, F. Qin, J. Bao, M. J. Yacaman, P. M. Ajayan, D. Chen and J. M. Tour, *Nat. Commun.*, 2015, **6**, 8668.
- W. Liu, L. Zhang, W. Yan, X. Liu, X. Yang, S. Miao, W. Wang, A. Wang and T. Zhang, *Chem. Sci.*, 2016, **7**, 5758.
- X.-F. Yang, A. Wang, B. Qiao, J. Li, J. Liu and T. Zhang, *Acc. Chem. Res.*, 2013, **46**, 1740.
- J. Liu, *ACS Catal.*, 2016, **7**, 34.
- W. Liu, Y. Chen, H. Qi, L. Zhang, W. Yan, X. Liu, X. Yang, S. Miao, W. Wang, C. Liu, A. Wang, J. Li and T. Zhang, *Angew. Chem., Int. Ed.*, 2018, **57**, 7071.
- Q. Cheng, S. Han, K. Mao, C. Chen, L. Yang, Z. Zou, M. Gu, Z. Hu and H. Yang, *Nano Energy*, 2018, **52**, 485.
- W. Ju, A. Bagger, G.-P. Hao, A. S. Varela, I. Sinev, V. Bon, B. Roldan Cuenya, S. Kaskel, J. Rossmeisl and P. Strasser, *Nat. Commun.*, 2017, **8**, 944.
- H. B. Yang, J. Miao, S.-F. Hung, J. Chen, H. B. Tao, X. Wang, L. Zhang, R. Chen, J. Gao, H. M. Chen, L. Dai and B. Liu, *Sci. Adv.*, 2016, **2**, e1501122.
- M. Wang, M. Lin, J. Li, L. Huang, Z. Zhuang, C. Lin, L. Zhou and L. Mai, *Chem. Commun.*, 2017, **53**, 8372.
- H. B. Yang, S.-F. Hung, S. Liu, K. Yuan, S. Miao, L. Zhang, X. Huang, H.-Y. Wang, W. Cai, R. Chen, J. Gao, X. Yang, W. Chen, Y. Huang, H. M. Chen, C. M. Li, T. Zhang and B. Liu, *Nat. Energy*, 2018, **3**, 140.
- W. Yang, X. Liu, X. Yue, J. Jia and S. Guo, *J. Am. Chem. Soc.*, 2015, **137**, 1436.
- B. J. Tan, K. J. Klabunde and P. A. Sherwood, *J. Am. Chem. Soc.*, 1991, **113**, 855.
- F. Cheng, T. Zhang, Y. Zhang, J. Du, X. Han and J. Chen, *Angew. Chem., Int. Ed.*, 2013, **52**, 2474.
- J. Meng, C. Niu, L. Xu, J. Li, X. Liu, X. Wang, Y. Wu, X. Xu, W. Chen, Q. Li, Z. Zhu, D. Zhao and L. Mai, *J. Am. Chem. Soc.*, 2017, **139**, 8212.
- A. Zitolo, V. Goellner, V. Armel, M.-T. Sougrati, T. Mineva, L. Stievano, E. Fonda and F. Jaouen, *Nat. Mater.*, 2015, **14**, 937.
- C. Tang, B. Wang, H.-F. Wang and Q. Zhang, *Adv. Mater.*, 2017, **29**, 1703185.
- L. Zhu, D. Zheng, Z. Wang, X. Zheng, P. Fang, J. Zhu, M. Yu, Y. Tong and X. Lu, *Adv. Mater.*, 2018, **30**, 1805268.
- H. Cheng, J. M. Chen, Q. J. Li, C. Y. Su, A. N. Chen, J. X. Zhang, Z. Q. Liu and Y. X. Tong, *Chem. Commun.*, 2017, **53**, 11596.